Detection prospects for Majorana fermion WIMPless dark matter

Keita Fukushima, Jason Kumar, and Pearl Sandick

Phys. Rev. D **84**, 014020 — Published 19 July 2011

DOI: 10.1103/PhysRevD.84.014020

UH-511-1166-2011, UTTG-06-11, TCC-008-11

Detection Prospects for Majorana Fermion WIMPless Dark Matter

Keita Fukushima,[1] Jason Kumar,[1] and Pearl Sandick[2]

[1] *Department of Physics and Astronomy, University of Hawai'i, Honolulu, HI 96822, USA*

[2] *Theory Group and Texas Cosmology Center, The University of Texas at Austin, TX 78712, USA*

Abstract

We consider both velocity-dependent and velocity-independent contributions to spin-dependent (SD) and spin-independent (SI) nuclear scattering (including one-loop corrections) of WIMPless dark matter, in the case where the dark matter candidate is a Majorana fermion. We find that spin-independent scattering arises only from the mixing of exotic squarks, or from velocity-dependent terms. Nevertheless (and contrary to the case of MSSM neutralino WIMPs), we find a class of models which cannot be detected through SI scattering, but can be detected at IceCube/DeepCore through SD scattering. We study the detection prospects for both SI and SD detection strategies for a large range of Majorana fermion WIMPless model parameters.

PACS numbers: 14.65.Jk, 13.85.Rm, 95.35.+d

I. INTRODUCTION

WIMPless dark matter [1, 2] is a versatile scenario in which the dark matter candidate is a hidden sector particle whose mass is at the hidden sector soft SUSY-breaking scale. The central feature of this scenario is that the dark matter candidate is a thermal relic which naturally has approximately the correct relic density to explain cosmological evidence of dark matter. This is a very robust result which is essentially determined by dimensional analysis, and does not depend on the details of the hidden sector. WIMPless dark matter models thus provide a wealth of detection signatures which differ significantly from typical WIMP models, spanning a wide range of dark matter masses (for either a bosonic or fermionic dark matter candidate).

WIMPless dark matter couples to Standard Model matter multiplets through Yukawa couplings to a 4th generation multiplet, yielding signals observable by direct detection experiments, through indirect detection, and at colliders. A variety of interesting signatures of WIMPless dark matter have been studied in the case where the candidate is a scalar [3–8], with a particular focus on the limit of low mass and large spin-independent scattering cross-section ($\sigma_{\rm SI}$), i.e., the region of parameter-space nominally preferred by the data from the DAMA, CoGeNT and CRESST experiments [9]. These include signatures from direct detection experiments [3, 5, 8], hadron colliders [6], neutrino detectors [4], gamma ray measurements [3], measurements of invisible Υ-decays at B-factories and new contributions to $b-s$ mixing [5].

But there are other interesting examples of WIMPless dark matter that provide very different detection signatures which will soon be probed by experiments. One of the most interesting cases is when the WIMPless dark matter candidate is a Majorana fermion. In this case, the tree-level scattering cross-section can have both spin-dependent ($\sigma_{\rm SD}$) and spin-independent ($\sigma_{\rm SI}$) components. While it is possible for scattering to be entirely spin-dependent, it cannot be entirely spin-independent.

Dark matter detection experiments can be sensitive to $\sigma_{\rm SI}$ and/or $\sigma_{\rm SD}$. The best experimental sensitivity to both types of scattering is for dark matter mass $m_X \sim \mathcal{O}(100)$ GeV. For this mass scale, direct detection experiments like SuperCDMS, XENON 100/1T and LUX are expected to provide the best sensitivity to $\sigma_{\rm SI}$, while neutrino experiments like

IceCube/DeepCore are expected to have the best sensitivity to $\sigma_{\rm SD}$[1]. Typically, direct detection experiments are much more sensitive to $\sigma_{\rm SI}$, due to the A^2 enhancement arising from coherent nuclear scattering. As a result, current bounds on $\sigma_{\rm SI}$ are roughly 4 orders of magnitude tighter than those for $\sigma_{\rm SD}$, and future experimental sensitivity to $\sigma_{\rm SI}$ is expected to far exceed sensitivity to $\sigma_{\rm SD}$. Indeed, experimental sensitivity to even velocity-suppressed spin-independent couplings can rival sensitivity to spin-dependent couplings [10]. For many dark matter models, this implies that $\sigma_{\rm SI}$ is most relevant for detection.

For the MSSM, a scan of parameters (without the assumption of gaugino mass unification) has found models for which $\sigma_{\rm SD}$ can potentially be measured, but for which velocity-independent contributions to $\sigma_{\rm SI}$ are too small to be detected with current or future experiments [11]. However, such models tend to be focused at low-mass; the scan in [11] did not find any such models with $m_X \gtrsim 200$ GeV. Since the couplings of the MSSM dictate the relative contribution of Higgs, Z, squark and axion exchange to neutralino-nucleon scattering, it is difficult to entirely decouple spin-dependent couplings from spin-independent couplings. Moveover, MSSM models that exhibit spin-dependent scattering will also exhibit velocity-dependent spin-independent scattering; models which can be detected through spin-dependent scattering at current direct detection experiments can also be detected through even velocity-suppressed spin-independent scattering at direct detection experiments operating now or in the near future [10].

But for WIMPless dark matter, potential dark matter-nucleon interactions are more limited (exchange of a 4th generation multiplet). For Majorana fermion WIMPless models, the spin-dependent and spin-independent interactions can be decoupled for a wide range of dark matter mass. Since these models can have very small or vanishing $\sigma_{\rm SI}$, it is quite possible that for many such models, the key to detection is spin-dependent scattering. Detection prospects for Majorana fermion WIMPless dark matter thus depend sensitively on the interplay between spin-dependent and spin-independent contributions to dark matter-nucleus scattering.

In this paper, we consider the detection prospects for Majorana fermion WIMPless dark matter through both spin-dependent and spin-independent scattering. In section II, we

[1] The sensitivity of neutrino detectors to dark matter annihilation products depends, of course, on the branching fractions to different Standard Model final states.

describe the interactions of Majorana fermion WIMPless dark matter, in section III we review current and future experimental sensitivity to dark matter-nucleon scattering, in section IV we describe detection prospects for Majorana fermion WIMPless dark matter, and we conclude in section V.

II. INTERACTIONS OF MAJORANA FERMION WIMPLESS DARK MATTER

The WIMPless dark matter candidate is a hidden sector particle (X) at the hidden sector soft SUSY-breaking scale. The main feature of these models is that $g_X^2/m_X \sim g_{weak}^2/m_{weak}$, where g_X is the hidden sector gauge coupling, and m_X is the dark matter mass. Since $\langle \sigma_{ann.} v \rangle \propto (g^4/m^2)$, the WIMPless dark matter candidate has roughly the same annihilation cross-section as a WIMP, implying that the WIMPless candidate has approximately the correct relic density. A simple implementation of this model arises in gauge-mediated SUSY-breaking[2], where both the hidden sector and MSSM sector receive the effects of SUSY-breaking from a common SUSY-breaking sector. Both the MSSM and hidden sector soft scales are related to their gauge couplings by the vevs of the same spurion field, $\langle \Phi \rangle = M + \theta^2 F$, through the relation

$$\frac{g_X^2}{m_X}, \frac{g_{weak}^2}{m_{weak}} \propto \frac{M}{F}. \tag{1}$$

The case where the dark matter candidate is a Majorana fermion has previously been discussed in [13]. Majorana fermion WIMPless dark matter couples to Standard Model quarks through the Yukawa couplings

$$V = \lambda_{Li}(\bar{X} P_L q_i)\tilde{Y}_L + \lambda_{Ri}(\bar{X} P_R q_i)\tilde{Y}_R + h.c. \tag{2}$$

where q_i are MSSM quarks and i is a flavor index. The WIMPless dark matter candidate, X, is neutral under Standard Model symmetries; it is charged only under the hidden sector symmetry that stabilizes it (for simplicity, this symmetry is assumed to be discrete). The $\tilde{Y}_{L,R}$ are exotic scalar connector particles which are charged under both the MSSM and the hidden sector symmetry. Gauge-invariance thus implies that the $\tilde{Y}_{1,2}$ are in a 4th generation quark multiplet.

[2] WIMPless models can also be constructed in the context of anomaly-mediated supersymmetry-breaking [12].

The $\tilde{Y}_{L,R}$ need not be mass eigenstates. In general, the mass eigenstates $\tilde{Y}_{1,2}$ are related to $\tilde{Y}_{L,R}$, through the mixing angle, α;

$$\begin{aligned}\tilde{Y}_L &= \tilde{Y}_1 \cos\alpha + \tilde{Y}_2 \sin\alpha \\ \tilde{Y}_R &= -\tilde{Y}_1 \sin\alpha + \tilde{Y}_2 \cos\alpha. \end{aligned} \tag{3}$$

If the dark matter candidate is a Majorana fermion, then the above Yukawa couplings permit scattering from Standard Model quarks via tree-level s- or u-channel exchange of the 4th generation squarks, $\tilde{Y}_{L,R}$. The dark matter candidate, X, can also annihilate to Standard Model particles through exchange of a 4th generation multiplet.

In [13], it was assumed that the 4th generation squarks $\tilde{Y}_L$ and $\tilde{Y}_R$ did not mix, but this need not be true. Assuming $m_{\tilde{Y}_1} < m_{\tilde{Y}_2}$, dark matter-nucleon scattering is mediated by the effective operator

$$\begin{aligned}\mathcal{O} &= \alpha_{1i}(\bar{X}\gamma^\mu\gamma^5 X)(\bar{q}_i\gamma_\mu q_i) + \alpha_{2i}(\bar{X}\gamma^\mu\gamma^5 X)(\bar{q}_i\gamma_\mu\gamma^5 q_i) + \alpha_{3i}(\bar{X}X)(\bar{q}_i q_i) \\ &\quad + \alpha_{4i}(\bar{X}\gamma^5 X)(\bar{q}_i\gamma^5 q_i) + \alpha_{5i}(\bar{X}X)(\bar{q}_i\gamma^5 q_i) + \alpha_{6i}(\bar{X}\gamma^5 X)(\bar{q}_i q_i), \end{aligned} \tag{4}$$

with

$$\begin{aligned}\alpha_{1i} &= \left[\frac{|\lambda_{Li}^2|}{8}\left(\frac{\cos^2\alpha}{m_{\tilde{Y}_1}^2 - m_X^2} + \frac{\sin^2\alpha}{m_{\tilde{Y}_2}^2 - m_X^2}\right) - \frac{|\lambda_{Ri}^2|}{8}\left(\frac{\cos^2\alpha}{m_{\tilde{Y}_2}^2 - m_X^2} + \frac{\sin^2\alpha}{m_{\tilde{Y}_1}^2 - m_X^2}\right)\right] \\ \alpha_{2i} &= \frac{|\lambda_{Li}^2|}{8}\left(\frac{\cos^2\alpha}{m_{\tilde{Y}_1}^2 - m_X^2} + \frac{\sin^2\alpha}{m_{\tilde{Y}_2}^2 - m_X^2}\right) + \frac{|\lambda_{Ri}^2|}{8}\left(\frac{\cos^2\alpha}{m_{\tilde{Y}_2}^2 - m_X^2} + \frac{\sin^2\alpha}{m_{\tilde{Y}_1}^2 - m_X^2}\right) \\ \alpha_{3i,4i} &= \frac{Re(\lambda_{Li}\lambda_{Ri}^*)}{4}(\cos\alpha\sin\alpha)\left[\frac{1}{m_{\tilde{Y}_1}^2 - m_X^2} - \frac{1}{m_{\tilde{Y}_2}^2 - m_X^2}\right] \\ \alpha_{5i,6i} &= \frac{\imath Im(\lambda_{Li}\lambda_{Ri}^*)}{4}(\cos\alpha\sin\alpha)\left[\frac{1}{m_{\tilde{Y}_1}^2 - m_X^2} - \frac{1}{m_{\tilde{Y}_2}^2 - m_X^2}\right] \end{aligned} \tag{5}$$

where we have used the notation of [14]. As shown there, α_2 is the coefficient of a pseudovector coupling which mediates spin-dependent scattering, while α_3 is the coefficient of a scalar coupling which mediates spin-independent scattering. These are the only couplings which are not velocity-suppressed. α_4 and α_5 are the coefficients of spin-dependent couplings which are also velocity-suppressed and will not be relevant for the detection prospects studied here. However, α_1 and α_6 are the coefficients of spin-independent couplings which are velocity-suppressed; though suppressed, the greater sensitivity of direct detection experiments to spin-independent couplings may make them relevant for detection purposes.

The dark matter-nucleus scattering cross-sections can then be written as

$$\begin{aligned}\sigma_{\rm SI} &= \sigma_{\rm SI}^{(1)} + \sigma_{\rm SI}^{(3)} + \sigma_{\rm SI}^{(6)} \\ \sigma_{\rm SD} &= \sigma_{\rm SD}^{(2)},\end{aligned} \tag{6}$$

with

$$\begin{aligned}\sigma_{\rm SI}^{(1)} &= \frac{4m_r^2}{\pi}\left[Z(\sum_i \alpha_{1i}B_i^p) + (A-Z)(\sum_i \alpha_{1i}B_i^n)\right]^2 \frac{v^2}{2} \\ \sigma_{\rm SI}^{(3)} &= \frac{4m_r^2}{\pi}\left[Z(\sum_i \alpha_{3i}B_i^p) + (A-Z)(\sum_i \alpha_{3i}B_i^n)\right]^2 \\ \sigma_{\rm SI}^{(6)} &= \frac{4m_r^2}{\pi}\left[Z(\sum_i \alpha_{6i}B_i^p) + (A-Z)(\sum_i \alpha_{6i}B_i^n)\right]^2 \frac{m_r^2 v^2}{2m_X^2} \\ \sigma_{\rm SD}^{(2)} &= \frac{16m_r^2}{\pi}\left[\sum_i \alpha_{2i}(\Delta_i^{(p)}\langle S_p\rangle + \Delta_i^{(n)}\langle S_n\rangle)\right]^2 \frac{J+1}{J}.\end{aligned} \tag{7}$$

Note that $\sigma_{\rm SI}^{(6)}$ is suppressed by an additional factor $(m_r/m_X)^2$, which is always less than 1. The integrated nuclear form factors are

$$B_u^p = B_d^n \simeq 12 \qquad B_d^p = B_u^n \simeq 6 \qquad B_s^{p,n} \simeq 4 \tag{8}$$

and we take the spin form factors to be [15]

$$\Delta_u^{(p)} = \Delta_d^{(n)} = 0.84 \qquad \Delta_d^{(p)} = \Delta_u^{(n)} = -0.43 \qquad \Delta_s^{(p,n)} = -0.09\,. \tag{9}$$

If dark matter couples largely to heavy quarks, then its scattering is largely spin-independent. Henceforth, we will focus on the case where the dark matter couples largely to the light quarks. We assume that the dominant couplings are to first generation quarks, and for simplicity, we will also assume $\lambda_{Ru} = \lambda_{Rd} = \lambda_R$.

The ratio of spin-independent to spin-dependent couplings is bounded from above by $\frac{\alpha_3}{\alpha_2} \leq \frac{1}{2}$, where the inequality is saturated in limit of real couplings with $\lambda_L = \lambda_R$, maximal mixing ($\alpha = \frac{\pi}{4}$) and $m_{\tilde{Y}_2} \to \infty$. This maximum value of σ_{SI}/σ_{SD} is obtained only outside the range of $\sigma_{\rm SI}$ and $\sigma_{\rm SD}$ considered here.

The analysis of [13] corresponds to the case where $\alpha_{1,3,6} = 0$. The dominant spin-independent coupling arises from α_3, and there are four limits in which $\alpha_3 \to 0$:

- $\lambda_L = 0$ (or $\lambda_R = 0$)
- $\alpha = 0$

- $m_{\tilde{Y}_1} = m_{\tilde{Y}_2}$
- maximal CP-violation ($\arg(\lambda_L \lambda_R^*) = \pm\frac{\pi}{2}$)

For the remainder of this work, we will focus on the case of real Yukawa couplings, i.e. no CP-violation. In these limits, spin-independent scattering is necessarily velocity-suppressed. But even these velocity-dependent terms can be made arbitrarily small. For example, in the limit

$$\alpha \to 0 \text{ and } \frac{|\lambda_L^2|}{(m_{\tilde{Y}_1}^2 - m_X^2)} = \frac{|\lambda_R^2|}{(m_{\tilde{Y}_2}^2 - m_X^2)} \tag{10}$$

one would have $\alpha_{1,3,6} \to 0$. In this limit, scattering detection prospects must rely entirely on detectors sensitive to $\sigma_{\rm SD}$. As one deviates from these limits, detectors sensitive to $\sigma_{\rm SI}$ can become relevant.

A. One-loop corrections

One should also consider one-loop scattering diagrams which could potentially generate spin-independent scattering. However, we shall find that in the case of Majorana fermion WIMPless dark matter these are not relevant to direct detection prospects.

We consider the limit where $\alpha \to 0$, since terms involving squark-mixing will yield spin-independent scattering even at tree-level. The only relevant one-loop scattering diagrams we can write involve s- or u-channel exchange of a squark, along with exchange of a photon or Z between the Standard Model fermion lines. Since we are considering models that couple to 1st generation quarks, the h, H and A exchange diagrams are highly suppressed. Assuming the squark exchanged is $\tilde{Y}_L$, the matrix element for the relevant one-loop diagrams is of the form

$$\mathcal{M} \propto g^2 \lambda_L^2 \int \frac{d^4p}{(2\pi)^4} \langle Xf|[\bar{X} P_L (\not{p} + m_f)\gamma^\mu f][\bar{f}\gamma_\mu (\not{p} - m_f) P_R X]|Xf\rangle f_0(p), \tag{11}$$

where the factor $f_0(p)$ contains the momentum dependence of the propagators in the loop diagram. Note that the terms proportional to $g^2 m_f^2$ will be heavily suppressed compared to the tree-level terms, and can be dropped. Furthermore, the matrix element will be of this form regardless of whether a photon or Z is exchanged; an additional γ^5 factor at one or more interaction vertices will not change the matrix element except by an overall sign, since

$\gamma^5 P_{L,R} = \pm P_{L,R}$. We then find

$$\begin{aligned}\mathcal{M} &\propto g^2\lambda_L^2\langle Xf|(\bar{X}P_L\gamma^\nu\gamma^\mu f)(\bar{f}\gamma_\mu\gamma_\nu P_R X)|Xf\rangle \\ &= g^2\lambda_L^2\langle Xf|(\bar{X}P_L f)(\bar{f}P_R X)|Xf\rangle - 2g^2\lambda_L^2\langle Xf|(\bar{X}\sigma^{\mu\nu}P_L f)(\bar{f}\sigma_{\mu\nu}P_R X)|Xf\rangle. \quad (12)\end{aligned}$$

After a Fierz transformation, the second term in brackets can be shown to vanish. The first term in brackets is a pseudovector coupling, and therefore corresponds to a loop-correction to $\sigma_{\rm SD}$, which is irrelevant for our purposes. We thus see that there are no relevant one-loop contributions to $\sigma_{\rm SI}$, and spin-independent scattering arises only from squark-mixing and velocity-suppressed contributions.

III. CURRENT AND PROSPECTIVE BOUNDS ON σ_{SI} AND σ_{SD}

We now briefly review some of the detectors which are relevant to current and future bounds on (sensitivities to) $\sigma_{\rm SI}$ and $\sigma_{\rm SD}$. These detection bounds arise from direct detection experiments, neutrino experiments, and also from colliders. Direct detection experiments measure the energy of a nucleus recoiling from a dark matter interaction, whereas neutrino experiments search for the neutrino flux produced when two dark matter particles annihilate. Direct detection experiments are sensitive to both $\sigma_{\rm SI}$ and $\sigma_{\rm SD}$. Although neutrino experiments are also sensitive to $\sigma_{\rm SI}$, their sensitivity does not rival that of direct detection experiments, whose sensitivity to $\sigma_{\rm SI}$ is enhanced by coherent scattering of the heavy nuclei of the detector. But the sensitivity of neutrino experiments to $\sigma_{\rm SD}$ is very competitive with that of direct detection experiments.

The current leading bounds on $\sigma_{\rm SI}$ at $m_X = 100$ GeV are set by CDMS-II (Cryogenic Dark Matter Search II) [16] and XENON100 [17]. CDMS-II utilizes germanium (~ 4.4 kg) and silicon (~ 1.1 kg) detectors, and measures both ionization and phonon energy to distinguish signal events from background. XENON100 utilizes liquid xenon (62 kg fiducial mass), and similarly measures both ionization and scintillation yield to distinguish signal from background. Current bounds from XENON100 have been set using 11 days of data. At the time of publication, XENON100 is collecting data, and an upgrade to ~ 1000 kg fiducial mass (XENON1T) [18] is expected to begin operating around 2014. Meanwhile, SuperCDMS is expected to begin operation in 2013-2015, using a germanium detector with a target mass of 100 kg [19].

GeODM 1.5T (Germanium Observatory for Dark Matter) will detect ionization and phonons in a $\sim$ 1500 kg fiducial mass germanium target [20], and is expected to begin operating in 2017-2021.

The LUX (Large Underground Xenon) experiment is also a liquid xenon-based detector, with a 350 kg fiducial mass [21]. This detector is expected to begin operation in 2011. In conjunction with ZEPLIN (Zoned Proportional scintillation in LIquid Noble gases), upgrades to a fiducial mass of 3000 kg (LUX-ZEP 3T) and, finally, 20000 kg (LUX-ZEP 20T), are planned for the next several years [21].

The DEAP/CLEAN family of detectors are purely liquid-phase noble gas scintillation detectors utilizing either neon or argon. MiniCLEAN (Cryogenic Low Energy Astrophysics with Noble gases) runs with either $\sim$ 100 kg fiducial mass of liquid argon or $\sim$ 85 kg fiducial mass of liquid neon as the target [22]. It is expected to be installed at SNOLAB this year. DEAP-3600 (Dark matter Experiment in Argon using Pulse-shape discrimination) is a liquid argon detector with $\sim$ 1000 kg fiducial mass, also expected to be installed at SNOLAB this year [23].

LUX-ZEP 20T would have the greatest sensitivity to $\sigma_{\rm SI}$ obtainable from a zero-background direct detection experiment ($\sim 10^{-12}$ pb). For smaller cross-sections, neutrino-nucleus scattering becomes a significant and irreducible background [24].

Significant bounds on spin-dependent scattering are obtained from both direct detection experiments and from neutrino detectors searching for dark matter annihilation in the sun. The best current bound on $\sigma^p_{\rm SD}$ from a direct detection experiment at $m_X = 100$ GeV is from SIMPLE (Superheated Instrument for Massive ParticLe Experiments) [25], which consists of superheated droplet detectors made of C_2ClF_5 droplets in a gel matrix. COUPP (Chicagoland Observatory for Underground Particle Physics) [26], which uses a bubble chamber filled with 3.5kg of CF_3I to search for dark matter nuclear recoils while rejecting electron recoil events, is also competitive. The best current bound on $\sigma^n_{\rm SD}$ from a direct detection experiment at $m_X = 100$ GeV comes from XENON10 [27], the precursor to XENON100.

Improved bounds on $\sigma^p_{\rm SD}$ are possible with DMTPC (Dark Matter Time Projection Chamber), a CF_4 gas scintillator. DMTPC currently operates with a 10 L fiducial volume [28], but it is anticipated that DMTPC will be upgraded to a 1 m^3 fiducial volume (DMTPC-ino), with a further possible upgrade to Large DMTPC with $10^2 - 10^3$ kg fiducial mass [28, 29].

Super-Kamiokande is a 22.5 kT water Chernekov detector and can detect charged-current

interactions of neutrinos arising from dark matter annihilation in the Sun [30]. It has accumulate over 3000 live-days of data already. Similarly, IceCube uses ~ 1 km^3 of deep and ultra-transparent Antarctic ice as a Cherenkov detector of neutrinos [31]. The DeepCore extension to IceCube includes a denser array of digital optical modules, whose installation was completed in January 2010. This denser array allows IceCube/DeepCore to be sensitive to lower-mass dark matter ($m_X > 35$ GeV). One should note that the sensitivity of neutrino detectors to $\sigma_{\rm SD}$ is somewhat model-dependent, and in particular depends on the dark matter annihilation channel. The Super-Kamiokande bound assumes dark matter annihilation to b-quarks. The prospective IceCube/DeepCore sensitivity cited here is the "hard" channel reported by IceCube/DeepCore, which is the assumption of annihilation entirely to τ leptons for $m_X < 80$ GeV, and annihilation to W bosons for $m_X > 80$ GeV (although the bounds found in [13] are tighter than those reported in [31]), for 1800 live-days of data. The prospective bounds from these neutrino detectors are only relevant here if the dark matter candidate has a significant annihilation branching fraction to heavy particles. This is certainly reasonable, as the WIMPless candidate is a Majorana fermion, so the cross section for annihilation to light fermions is chirality suppressed.

Collider experiments, such as the Tevatron and Large Hadron Collider (LHC) can also constrain the dark matter-nucleon scattering cross section [32, 33][3]. The effective operators in eq. 4 allow two quarks to annihilate to dark matter, which contributes to the process $p\bar{p}(pp) \to XX + jets$, where the jets arise from initial state radiation. Collider searches for this process can thus constrain the operator coefficients α_i.

CDF has performed monojet searches with 1 fb^{-1} of data [34]. The search looks for events with missing $p_T > 80$ GeV, a leading jet with $p_T > 80$ GeV, and the constraints that a second jet (if present) must have $p_T < 30$ GeV and that there be no other jets with $p_T > 20$ GeV. This search bounds the new physics contribution to this signature at $\sigma_{NP} < 0.664$ pb at the 2σ-confidence level. If one assumes that only α_3 is non-zero, the CDF bound on α_3 corresponds to a bound on $\sigma_{\rm SD}$ (for $m_X \sim 100$ GeV, similar constraints on the effective operators contributing to spin-independent scattering are not competitive with

[3] Note that the analysis of [33] assumes that the pseudovector coupling of dark matter is flavor-independent, whereas we are considering WIMPless models which couple only to first generation quarks. We expect that the coupling of dark matter to second and third generation quarks has a negligible effect on collider sensitivity to the pseudovector coupling.

bounds from direct detection experiments). Tevatron bounds on this pseudovector exchange effective operator are quite stringent [33].

In [33], the ability of the LHC to probe the pseudovector exchange scattering operator with 100 fb^{-1} of data was also studied. This studied assumed a signal of jets and missing $p_T > 500$ GeV, where the background was determined from [35]. The sensitivity of the LHC to this operator will be very competitive with that from direct detection and neutrino experiments.

However, as with neutrino experiments, the bounds from collider experiments are also somewhat model-dependent. In particular, these bounds assume the validity of the effective operator analysis at collider energies. These bounds are strictly valid in the limit where the exotic squark masses $m_{\tilde{Y}1,2}$ are much larger energy of the hard scattering process; if the squark masses are comparable to collider energies, these bounds can be weakened.

IV. DETECTION PROSPECTS

In this section, we present the results of a WIMPless dark matter parameter space scan, followed by an analysis of the three limits described in Section II in which $\sigma_{\rm SI} \to 0$ (neglecting the limit of maximal CP-violation).

Figure 1 shows $\sigma_{\rm SI}$ and $\sigma_{\rm SD}$ for a scan of the parameter space of Majorana fermion WIMPless dark matter, where the parameters scanned over are

$$\begin{aligned} 0 \leq \alpha &\leq \pi/4 \\ 0 \leq \lambda_{L,R} &\leq \sqrt{4\pi} \\ 300\,\text{GeV} < m_{\tilde{Y}_1} &< 2\,\text{TeV} \\ m_{\tilde{Y}_1} < m_{\tilde{Y}_2} &< 2\,\text{TeV} \end{aligned} \tag{13}$$

and we take $m_X = 100$ GeV. The scan includes 2×10^5 model points, though a significant fraction lie at larger $\sigma_{\rm SI}$ than is shown in Fig. 1. For the velocity-dependent terms in the cross-section, we approximate $v = 220$ km/s. In a more detailed calculation, one would convolve the cross-section against a velocity distribution to determine an event rate at any given experiment, which in turn would determine the sensitivity at that experiment. Our approximation is sufficient for the purpose here, and allows us to determine the sensitivity of

any given experiment to Majorana fermion WIMPless dark matter using publicly available bounds.

We note that the priors for this scan are linear in α, $\lambda_{L,R}$ and $m_{\tilde{Y}_{1,2}}$. The current limits and projected sensitivities of direct detection experiments for $\sigma_{\rm SI}$ are shown as vertical lines, and those for $\sigma_{\rm SD}$ are shown as horizontal lines. The region of the plane above the horizontal solid blue line is currently excluded by non-observation of spin-dependent scattering on neutrons by XENON10 (the limit on $\sigma^p_{\rm SD}$ from SIMPLE is shown in red), while the region of the plane to the right of the vertical solid red line is excluded by non-observation of spin-independent scattering by CDMS-II and XENON10. Spin-(in)dependent cross sections above (to the right of) a particular sensitivity will be probed by the corresponding experiment.

Because of the greater sensitivity to $\sigma_{\rm SI}$ of detectors such as SuperCDMS, XENON1T and LUX, most models in this scan either have already been excluded, or can be detected through spin-independent scattering by future searches. The dominant contribution to spin-independent scattering is the velocity-independent term $\sigma^{(3)}_{\rm SI}$. The velocity-dependent terms $\sigma^{(1,6)}_{\rm SI}$ are suppressed by ~ 6 orders of magnitude, and only become relevant to detection prospects in regions of parameter space where $\sigma^{(3)}_{\rm SI} \sim 0$. Nevertheless, there are some models which cannot be detected through $\sigma_{\rm SI}$ with currently planned detectors, but can be detected through $\sigma_{\rm SD}$ at IceCube/DeepCore, or at the LHC[4]. These models lie above the cyan dashed IceCube/DeepCore sensitivity line (or the cyan dotted LHC sensitivity line), and at very low $\sigma_{\rm SI}$. Note, however, that the collider bounds from the Tevatron and the LHC (dotted lines) are only strictly valid in the limit where the squark mass is much larger than the collider energy scale. This will be true for models $m_{\tilde{Y}_{1,2}} \sim 2$ TeV, but some of these collider bounds can be substantially weakened if the squarks are lighter.

In Fig. 2, we present the behavior of $\sigma_{\rm SI}$ and $\sigma_{\rm SD}$ as we relax each of the three cases in which $\sigma_{\rm SI} \to 0$. We can parameterize each of these limits by a small parameter, which goes to zero as $\sigma_{\rm SI} \to 0$. These small parameters are λ_R, α, and $\delta = (m_{\tilde{Y}_2} - m_{\tilde{Y}_1})/m_{\tilde{Y}_1}$. As a benchmark, we consider $m_X = 100$ GeV, and $m_{\tilde{Y}_1} = 500$ GeV ($m_{\tilde{Y}_1} < m_{\tilde{Y}_2}$).

In the top panels of Fig. 2, we examine the limit $\lambda_R \to 0$, for maximal mixing, $\delta = 0.01$, and $\lambda_L = 0.44$. For these parameter choices, $\lambda_R \lesssim 0.065$ pushes $\sigma_{\rm SI}$ below the current

[4] Sensitivities of neutrino and collider experiments to $\sigma_{\rm SD}$ are shown as dashed and dotted lines, respectively, in Figs. 1-3.

bounds, while $\sigma_{\rm SD}$ is still large enough that the LHC might be sensitive to it. For $\lambda_L = 0.6$ however, and all other parameters fixed, one obtains $\sigma_{\rm SD}$ large enough to be detected by IceCube for $\lambda_R \gtrsim 0.08$, but all $\lambda_R \gtrsim 0.04$ are already excluded by non-observation of spin-independent scattering. For a model to be visible at IceCube but to have evaded the current constraint on $\sigma_{\rm SI}$, $\lambda_L \gtrsim 0.605$, for these parameters, including maximal mixing. If the mixing is not maximal and $\alpha < \pi/4$, viable models may have smaller λ_L and larger λ_R.

From the top right panel of Fig. 2, as from the shape of the contour in the left panel, it is clear that both $\sigma_{\rm SI}$ and $\sigma_{\rm SD}$ increase with λ_R, though $\sigma_{\rm SI}$ is more sensitive to changes in λ_R for small λ_R. Both $\sigma_{\rm SI}$ and $\sigma_{\rm SD}$ are sensitive to λ_L as well; $\sigma_{\rm SI}$ is approximately proportional to λ_L^2, but $\sigma_{\rm SD} \propto \lambda_L^4$ for $\lambda_L \ll \lambda_R$ and is dominated by λ_R for $\lambda_R \gg \lambda_L$.

Turning to the middle row of panels in Fig. 2, we examine the dependence on the mixing angle, α, for $\delta = 0.01$ and $\lambda_L = \lambda_R = 0.44$. In both panels in the middle row it is clear that $\sigma_{\rm SD}$ is independent of α. From equation 4, we see that $\sigma_{\rm SD}$ is independent of α for $\lambda_L = \lambda_R$ and/or $m_{\tilde{Y}_1} = m_{\tilde{Y}_2}$, both of which are satisfied for the choice of parameters here. $\sigma_{\rm SI}$, by contrast, changes rapidly at small mixing angles. Again, increasing the Yukawa couplings increases both $\sigma_{\rm SD}$ and $\sigma_{\rm SI}$. For the particular parameter choices here, the current bound on $\sigma_{\rm SI}$ is evaded for $\alpha \lesssim 0.08$.

In the bottom row of panels in Fig. 2, we assume maximal mixing ($\alpha = \pi/4$) and $\lambda_L = \lambda_R = 0.1$, and examine the departure from degeneracy of the squark masses (assuming $\delta > 0$). For this choice of parameters, we see from the bottom panel on the left that $\delta \lesssim$ few $\times 10^{-2}$ is necessary to evade current bounds on $\sigma_{\rm SI}$; however $\sigma_{\rm SD}$ is very small for Yukawa couplings in this range and will not be probed, even at the LHC. In the right panel, one can see that the primary effect of increasing δ is to increase $\sigma_{\rm SI}$, while $\sigma_{\rm SD}$ decreases slightly. It is possible to have much larger $\sigma_{\rm SD}$ and $\sigma_{\rm SI}$ if the Yukawa couplings are much larger than $\lambda_L = \lambda_R = 0.1$. When the Yukawa couplings are increased, it is still possible to have $\sigma_{\rm SI}$ below current bounds, but a much smaller value of δ is required; for $\lambda_L = \lambda_R = 0.35$, $\sigma_{\rm SD}$ is within the IceCube sensitivity, but a squark mass non-degeneracy of $\delta \lesssim$ few $\times 10^{-3}$ is necessary so that $\sigma_{\rm SI}$ is not already excluded.

In Figure 3, we examine the possibility that there is no squark mixing ($\alpha = 0$). In this case, the spin-independent elastic scattering cross section is due entirely to the velocity-suppressed contributions $\sigma_{\rm SI}^{(1)}$ and $\sigma_{\rm SI}^{(6)}$. Since we have assumed real Yukawa couplings, $\sigma_{\rm SI}^{(6)} = 0$. We see from the figure that even for $\lambda_L \approx \lambda_R \approx 1$, $\sigma_{\rm SI}$ is well below the current constraints,

while $\sigma_{\rm SD}$ is quite large[5]. For $\epsilon > 0$, both $\sigma_{\rm SD}$ and $\sigma_{\rm SI}$ increase with ϵ, though only $\sigma_{\rm SI} \to 0$ rapidly as $\epsilon \to 0$. Here, $\epsilon \lesssim 0.008$ will result in dark matter that will be evident only through its spin-dependent scattering. All other parameters fixed, models can be visible at both IceCube and LUX/ZEP 20T with λ_L as small as 0.421, with $\epsilon > 0.045$ ($\lambda_R > 0.412$).

Finally, returning to the parameter scan in Fig. 1, of great interest are the regions of parameter space in which a discovery may be made by IceCube/DeepCore or the LHC, but which would evade all searches for spin-independent scattering on nuclei, namely those points with $\sigma_{\rm SD} \gtrsim 10^{-6}$ pb and $\sigma_{\rm SI} \lesssim 10^{-12}$ pb. These points are characterized by large $m_{\tilde{Y}_1}$ and $m_{\tilde{Y}_2}$ ($\gtrsim 1500$ GeV, near the edge of our range), one large Yukawa coupling ($\gtrsim 2$), and one small Yukawa coupling ($\lesssim 0.2$), *or* very nearly degenerate squark masses ($\delta \approx 0$) and two relatively large Yukawa couplings, *or* a combination of near-degeneracy of squark masses and large-ish Yukawa couplings. In the latter cases, small-ish α can also help induce a small $\sigma_{\rm SI}$ without reducing $\sigma_{\rm SD}$ due to the degeneracy of the squark masses. In the first case, if the small Yukawa is very small ($\lesssim 10^{-2}$), the the lighter squark can be as light as ~ 1 TeV, and the larger Yukawa does not necessarily have to be larger than 2.

This result is not unexpected; in the limit of small α and δ, $\frac{\alpha_3}{\alpha_2} \propto (\lambda_R/\lambda_L)^2 \alpha\delta$, so a scan with linear priors will favor the region of parameter-space with large Yukawa couplings and masses. Logarithmic priors would instead favor all mass and coupling scales equally. Given linear priors and the suppression needed to evade upcoming bounds on $\sigma_{\rm SI}$, the points we have generated which may be detected by spin-dependent scattering but which will evade detection by spin-independent scattering occur when at least two of the $\sigma_{\rm SI} \to 0$ criteria are approximately satisfied.

In this analysis, we have restricted the WIMPless dark matter mass to be $m_X = 100$ GeV due to the wealth of direct dark matter searches sensitive to this mass, however a similar analysis may be carried out for any m_X. Both $\sigma_{\rm SD}$ and $\sigma_{\rm SI}$ decrease for smaller m_X, but the changes to Fig. 1 are minor, with the exception of the relevant constraints. Indeed, the qualitative conclusions drawn from Figs. 2 and 3 are valid for any m_X.

[5] Note that $\sigma_{\rm SD}$ is only mildly dependent on ϵ, as evident in the right panel of Fig. 3. For the parameter choices in the left panel, none of the $\sigma_{\rm SD}$ experimental sensitivities are visible, though the range of $\sigma_{\rm SD}$ plotted here lies just below the Tevatron sensitivity (shown as a horizontal green dotted line in Fig. 1) and well-above the sensitivity of Large DMTPC and IceCube/DeepCore (shown as grey solid and cyan dashed lines, respectively, in Fig. 1).

V. CONCLUSION

We have considered the detection prospects for Majorana fermion WIMPless dark matter at current and near future dark matter detectors, using both spin-independent and spin-dependent scattering. We have found that although Majorana fermion WIMPless dark matter always exhibits spin-dependent nuclear scattering, spin-independent scattering contributions are always either velocity-dependent or dependent on mixing of exotic 4th generation squarks. One-loop corrections do not generate spin-independent contributions which could potentially be detected at upcoming experiments.

A scan of models shows that the majority of models which could be detected by IceCube/DeepCore (with 1800 live-days of data) or at the LHC can also be detected through spin-independent scattering by detectors such as SuperCDMS, XENON100 and DEAP/CLEAN (as well as the first generation LUX detector) over a comparable time frame. However, a significant fraction of models detectable at IceCube/DeepCore or the LHC would not be detected through spin-independent scattering until major future upgrades are made, if at all. Unlike the case of MSSM neutralino WIMPs, it is possible for WIMPless Majorana fermions which have evaded detection even through velocity-suppressed spin-independent scattering to nevertheless be detected by current detectors through spin-dependent scattering.

Acknowledgments

We gratefully acknowledge J. L. Feng for collaboration at an early stage of this project, and M. Felizardo, D. Marfatia and T. Tait for useful discussions. This work is supported in part by DOE grant DE-FG02-04ER41291. P.S. is supported by the National Science Foundation under Grant Numbers PHY-0969020 and PHY-0455649 and would also like to thank the University of Hawai'i for hospitality during the course of this research.

[1] J. L. Feng and J. Kumar, Phys. Rev. Lett. **101**, 231301 (2008) [arXiv:0803.4196 [hep-ph]].

[2] J. L. Feng, M. Kaplinghat, H. Tu and H. B. Yu, JCAP **0907**, 004 (2009) [arXiv:0905.3039 [hep-ph]].

[3] J. L. Feng, J. Kumar and L. E. Strigari, Phys. Lett. B **670**, 37 (2008) [arXiv:0806.3746 [hep-ph]];

[4] J. L. Feng, J. Kumar, J. Learned, L. E. Strigari, JCAP **0901**, 032 (2009). [arXiv:0808.4151 [hep-ph]].

[5] D. McKeen, Phys. Rev. **D79**, 114001 (2009). [arXiv:0903.4982 [hep-ph]];

[6] J. Alwall, J. L. Feng, J. Kumar and S. Su, Phys. Rev. D **81**, 114027 (2010) [arXiv:1002.3366 [hep-ph]];

[7] G. Zhu, [arXiv:1101.4387 [hep-ph]];

[8] J. L. Feng, J. Kumar, D. Marfatia, D. Sanford, [arXiv:1102.4331 [hep-ph]].

[9] R. Bernabei *et al.*, Eur. Phys. J. C **67**, 39 (2010) [arXiv:1002.1028 [astro-ph.GA]]; C. E. Aalseth *et al.* [CoGeNT collaboration], arXiv:1002.4703 [astro-ph.CO]; D. Hooper, J. I. Collar, J. Hall and D. McKinsey, arXiv:1007.1005 [hep-ph]; see talk of W. Seidel at IDM2010, `http://indico.in2p3.fr/contributionDisplay.py?contribId=195&sessionId=9&confId=1565`

[10] M. Freytsis and Z. Ligeti, arXiv:1012.5317 [hep-ph].

[11] E. Moulin, F. Mayet and D. Santos, Phys. Lett. B **614**, 143 (2005) [arXiv:astro-ph/0503436].

[12] J. L. Feng, Y. Shadmi, [arXiv:1102.0282 [hep-ph]].

[13] V. Barger, J. Kumar, D. Marfatia and E. M. Sessolo, Phys. Rev. D **81**, 115010 (2010) [arXiv:1004.4573 [hep-ph]]; J. Kumar, [arXiv:1012.0078 [hep-ph]].

[14] J. R. Ellis, J. L. Feng, A. Ferstl, K. T. Matchev and K. A. Olive, Eur. Phys. J. C **24**, 311 (2002) [arXiv:astro-ph/0110225]; J. Ellis, K. A. Olive and P. Sandick, New J. Phys. **11**, 105015 (2009) [arXiv:0905.0107 [hep-ph]].

[15] J. R. Ellis, K. A. Olive and C. Savage, Phys. Rev. D **77**, 065026 (2008) [arXiv:0801.3656 [hep-ph]].

[16] Z. Ahmed *et al.* [The CDMS-II Collaboration], Science **327**, 1619-1621 (2010). [arXiv:0912.3592 [astro-ph.CO]].

[17] E. Aprile *et al.* [XENON100 Collaboration], Phys. Rev. Lett. **105**, 131302 (2010) [arXiv:1005.0380 [astro-ph.CO]].

[18] E. Aprile *et al.*, arXiv:astro-ph/0207670.

[19] R. W. Schnee *et al.* [The SuperCDMS Collaboration], arXiv:astro-ph/0502435.

[20] P. Brink, 9th UCLA Symposium on Sources and Detection of Dark Matter and Dark Energy

in the Universe, 2010. www.physics.ucla.edu/hep/dm10/talks/brink.pdf.

[21] S. Fiorucci *et al.*, AIP Conf. Proc. **1200**, 977 (2010) [arXiv:0912.0482 [astro-ph.CO]].

[22] D. N. McKinsey [Mini-CLEAN Collaboration], Nucl. Phys. Proc. Suppl. **173**, 152-155 (2007).

[23] M. G. Boulay *et al.*, arXiv:0904.2930 [astro-ph.IM].

[24] L. E. Strigari, New J. Phys. **11**, 105011 (2009) [arXiv:0903.3630 [astro-ph.CO]].

[25] M. Felizardo *et al.*, Phys. Rev. Lett. **105**, 211301 (2010) [arXiv:1003.2987 [astro-ph.CO]]; T. Girard *et al.* [for the SIMPLE Collaboration], [arXiv:1101.1885 [astro-ph.CO]].

[26] E. Behnke, J. Behnke, S. J. Brice, D. Broemmelsiek, J. I. Collar, P. S. Cooper, M. Crisler, C. E. Dahl *et al.*, Phys. Rev. Lett. **106**, 021303 (2011). [arXiv:1008.3518 [astro-ph.CO]].

[27] J. Angle *et al.*, Phys. Rev. Lett. **101**, 091301 (2008) [arXiv:0805.2939 [astro-ph]].

[28] J. B. R. Battat *et al.*, arXiv:1012.3912 [astro-ph.IM].

[29] G. Sciolla *et al.*, J. Phys. Conf. Ser. **179**, 012009 (2009) [arXiv:0903.3895 [astro-ph.IM]].

[30] S. Desai *et al.* [Super-Kamiokande Collaboration], Phys. Rev. **D70**, 083523 (2004). [hep-ex/0404025].

[31] J. Braun and D. Hubert for the IceCube Collaboration, arXiv:0906.1615 [astro-ph.HE].

[32] J. L. Feng, S. Su, F. Takayama, Phys. Rev. Lett. **96**, 151802 (2006). [hep-ph/0503117].

[33] J. Goodman, M. Ibe, A. Rajaraman, W. Shepherd, T. M. P. Tait, H. -B. Yu, Phys. Lett. **B695**, 185-188 (2011). [arXiv:1005.1286 [hep-ph]].

[34] T. Aaltonen *et al.* [CDF Collaboration], Phys. Rev. Lett. **101**, 181602 (2008). [arXiv:0807.3132 [hep-ex]];
`http://www-cdf.fnal.gov/physics/exotic/r2a/20070322.monojet/public/ykk.html`

[35] L. Vacavant, I. Hinchliffe, J. Phys. G **G27**, 1839-1850 (2001).

[36] S. Fiorucci, "The LUX Dark Matter Search," Presentation at *Darkness Visible: Dark Matter in Astrophysics and Particle Physics*, Institute of Astronomy, University of Cambridge, UK, 2-6 August, 2010.

[37] R. Gaitskell, *et al.*, `http://dmtools.brown.edu/`

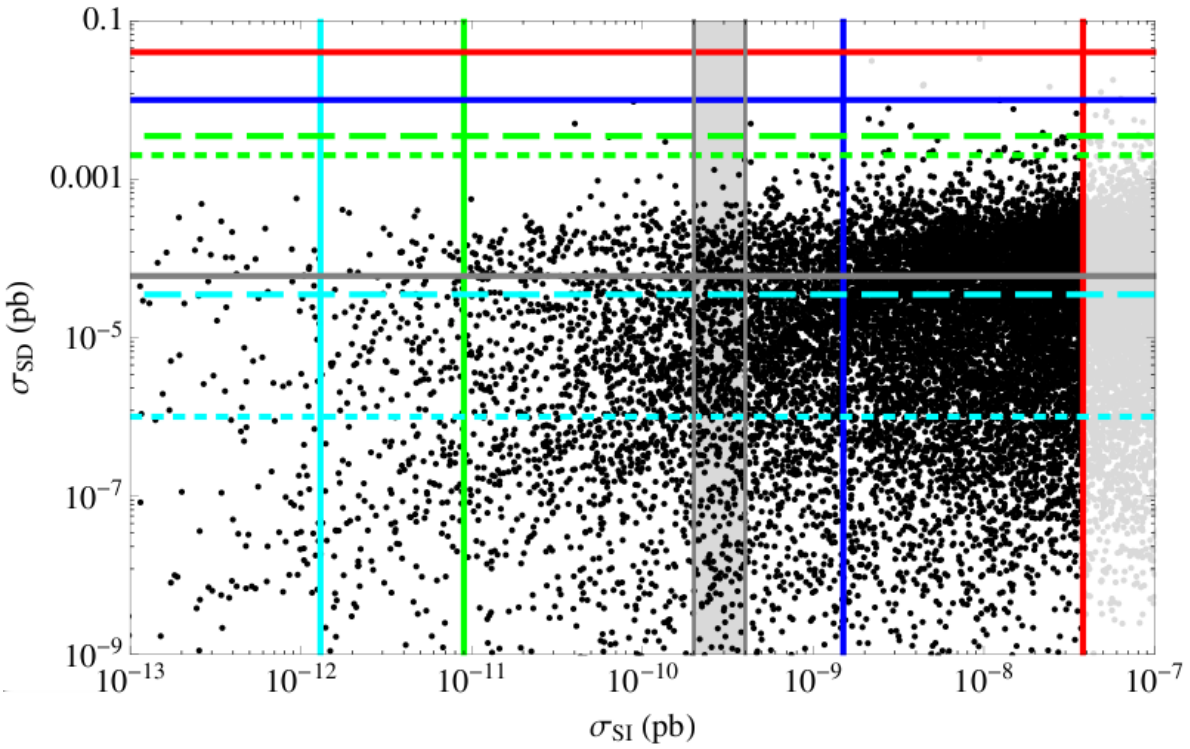

FIG. 1: Possible values of $\sigma_{\rm SI}$ and $\sigma_{\rm SD}$ for $0 \leq \lambda_L, \lambda_R \leq \sqrt{4\pi}$, $0 \leq \alpha \leq \frac{\pi}{4}$ and 300 GeV $< m_{\tilde{Y}_1} <$ 2 TeV, and $m_{\tilde{Y}_1} < m_{\tilde{Y}_2} <$ 2 TeV ($m_X = 100$ GeV). The dark (black) points represent viable models, the light (grey) points represent models that are ruled out by direct detection experiments. Also shown are the current limits and projected sensitivities of direct detection experiments for $\sigma_{\rm SI}$ (vertical lines) and $\sigma_{\rm SD}$ (horizontal lines). Constraints on $\sigma_{\rm SI}$ are (from right to left): the current limit from CDMS II [16] and XENON100 [17] (red solid); mini-CLEAN [37] (blue solid); the approximate sensitivity of SuperCDMS 100kg at SNOLAB [19], DEAP-3600 [37], XENON100 upgraded [17], and LUX with 300 days of exposure [36] (grey band); XENON1T [18] with 3 years of exposure (green solid), and LUX/ZEP 20T [37] (cyan solid). Constraints on $\sigma_{\rm SD}$ from direct detection experiments are shown as the solid lines (from top to bottom): the current limit from SIMPLE [25] (red solid) for scattering on protons; the current limit from XENON10 [27] (blue solid) for scattering on neutrons, and the projected sensitivity of Large DMTPC [29] (grey solid). Indirect constraints on $\sigma_{\rm SD}$ from neutrino experiments are shown as dashed lines: Super-Kamiokande [30] (green dashed); and the projected sensitivity of IceCube/DeepCore [31] with 1800 days of data (cyan dashed). The sensitivity to $\sigma_{\rm SD}$ of collider experiments, assuming contact interactions, is shown as dotted lines: the Tevatron [33] with 1 fb^{-1} of data (green dotted); and the projected sensitivity of the LHC [33] with 100 fb^{-1} of data (cyan dotted).

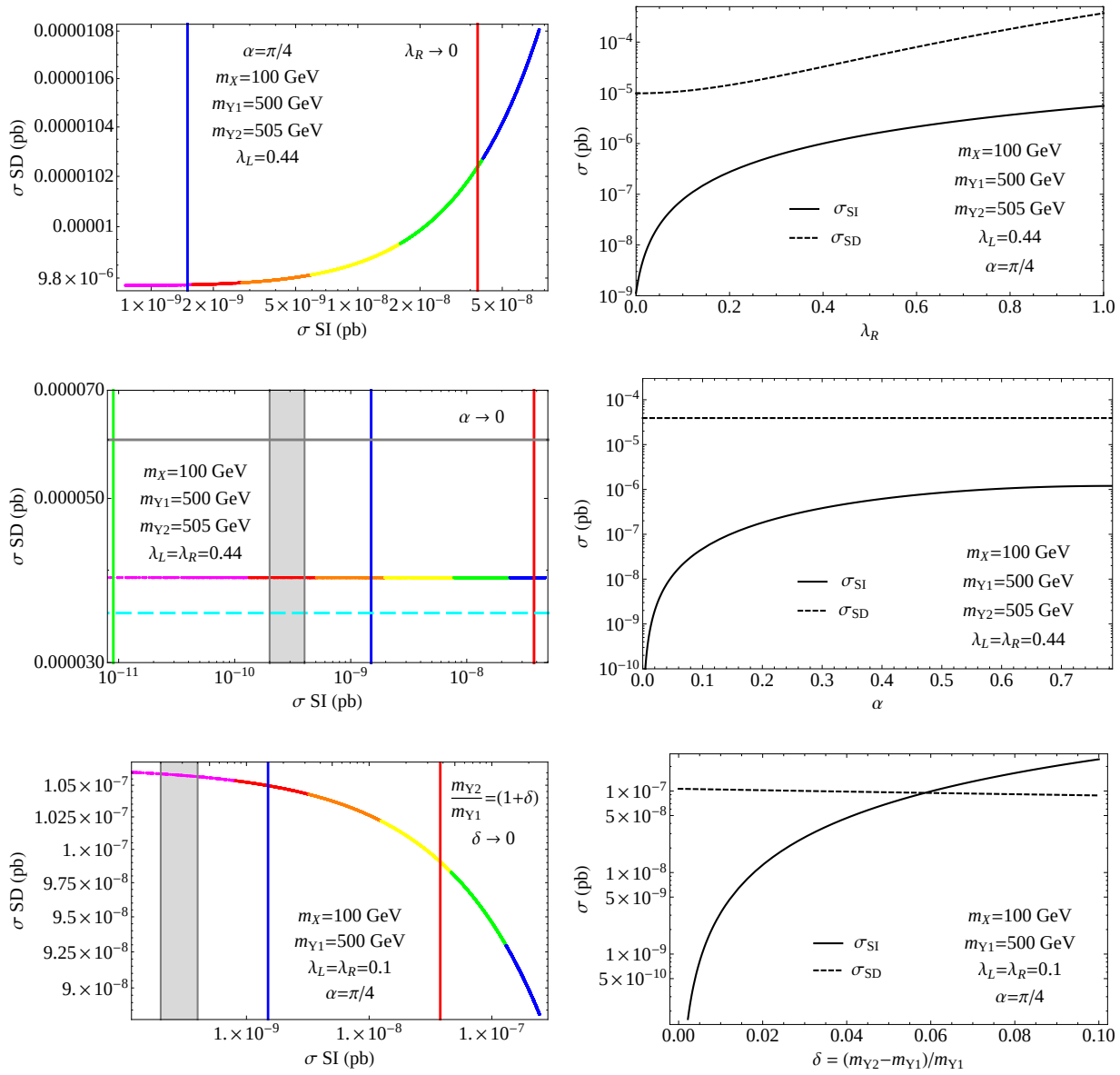

FIG. 2: Departures from the limiting cases where $\sigma_{\rm SI} \to 0$, as labeled in the upper right corner of the left panels (vertical and horizontal lines denote the same experimental sensitivities used in Fig. 1). In the left panels, we show the evolution in the $(\sigma_{\rm SI}, \sigma_{\rm SD})$ plane as the small parameter (λ_R, α, and δ, from top to bottom) is increased. The color coding indicates the value of the small parameter; 0 to 0.005 (magenta), 0.005 to 0.01 (red), 0.01 to 0.02 (orange), 0.02 to 0.04 (yellow), 0.04 to 0.07 (green), and 0.07 to 0.1 (blue). In the right panels, we show $\sigma_{\rm SD}$ (dashed curves) and $\sigma_{\rm SI}$ (solid curves) individually as functions of the small parameter.

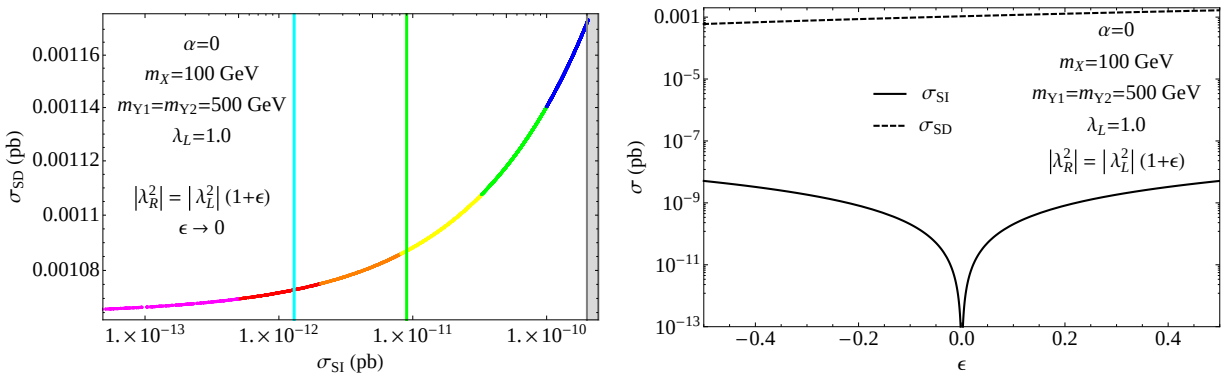

FIG. 3: Departure from the limiting cases where $\sigma_{\rm SI} \to 0$ due only to velocity-dependent terms (no squark mixing), as in Fig. 2. Again, horizontal lines denote the experimental sensitivities used in Fig. 1. In the left panels, we show the evolution in the $(\sigma_{\rm SI}, \sigma_{\rm SD})$ plane as ϵ, the spilitting between $|\lambda_L^2|$ and $|\lambda_R^2|$, is increased. The color coding indicates the value of ϵ; 0 to 0.005 (magenta), 0.005 to 0.01 (red), 0.01 to 0.02 (orange), 0.02 to 0.04 (yellow), 0.04 to 0.07 (green), and 0.07 to 0.1 (blue). In the right panel, we show $\sigma_{\rm SD}$ (dashed curves) and $\sigma_{\rm SI}$ (solid curves) individually as functions of ϵ.